PROCEEDINGS OF SCIENCE

Determination of the detection performances of the Euso-Balloon UV camera

Sylvie Dagoret-Campagne*, **Julio Arturo Rabanal Reina, Camille Moretto,Pierre Barrillon, Hiroko Miyamoto**†

Laboratoire de l'accélérateur linéaire, IN2P3,CNRS and University Paris-Sud
E-mail: dagoret@lal.in2p3.fr

Aera Jung, Simon Bacholle, Philippe Gorodetzky, Guillaume Prévôt

APC-Université Diderot, Paris 7

Sylvie Blin-Bondil

OMEGA, Ecole Polytechnique, IN2P3,CNRS

for the JEM-EUSO Collaboration

Recently, the Euso-Balloon instrument, the pathfinder for future space telescopes of the JEM-EUSO family, has been flown during one night in the stratosphere. The main goal of the mission was the recording of the light coming from the earth's surface by the fast and high-resolution UV camera on board of the balloon. We present an analysis of the in-flight UV camera calibration data. These data allow us the determination of the signal and background components in the recorded photoelectron count spectrum for each pixel based on a multi-component statistical model describing the experimental setup. We assess the detection performances i.e. the detection efficiency and sensitivity. We discuss as well the implication of this calibration for the statistical and systematic errors of the measurement of the photoelectron rates.

The 34th International Cosmic Ray Conference,
30 July- 6 August, 2015
The Hague, The Netherlands

*Speaker.
†On leave for Torino University, INFN

PoS(ICRC2015)607

1. Introduction

Euso-Balloon [1] is the first prototype implementing the full data chain of the future space telescope JEM-EUSO. It comprises all main components, from its optics to its data acquisition, including its challenging high performance UV camera. The camera utilises a special space-dedicated ASIC (Application Specific Integrated Circuit) for the processing of 64 pixels and a new miniaturised low power high voltage (HV) generator in a very dense and compact design. In a first balloon flight organised by the JEM-EUSO collaboration together with CNES[1], the camera was tested under the severe environmental conditions of the stratosphere (low pressure, low temperature). The whole camera succeeded in capturing UV images [2]. However, some flaws prevented the system to work at the optimal configuration. The main issues can be tracked through the detection performance parameters, which are presented in this analysis below. The method developed here allows us the prediction of the expected performances under the foreseen technical specifications, especially when a few identified technical problems will be solved for future balloon campaigns.

2. The Photo Detector Module

2.1 Overall description of the UV camera

The sensitive element of the camera is the Photo Detector Module (PDM), which consists of the following main components:

- the focal surface (15cm $\times$ 15cm), made up of an array of 6x6 Multi-Anode-Photomultipliers (MAPMT), each of 64 pixels (in total 2304 pixels). The MAPMT are fixed for mechanical stability in groups of 2x2 units, called Elementary Cells (EC-unit).
- The photocathodes are covered by absorption filters of BG3 glass. The whole EC-Unit has been potted to prevent High-Voltage sparking and breakdown in the low pressure environment of the stratosphere,
- Nine Cockroft-Walton High Voltage (HV) generators with their controller disposed in 4 boxes and also potted, provide each a set of 14 voltages (photocathode, grid, 12 dynodes voltages) required by each EC-Unit,
- The 64 anodes of a MAPMT are handled by a single ASIC chip. The 36 ASICS are placed on six double sided ASIC boards (6 ASIC per boards, 3 per side) called EC-ASICs,
- A master FPGA control board named the PDM-board collects the 64 8-bits numbers produced by each of the 36 ASICs in a period called a Gate Time Unit (1 $GTU = 2.5\mu$s).

2.2 The front-end electronic Scheme

The front end electronic scheme of a single channel is sketched in Figure 1.a). The MAPMT generates a current pulse in response to incoming light converted in the photo-cathode to photoelectrons (p.e.). The anode pulse is the result of the primary photoelectrons collection and their multiplication at the 12-dynode stages in random processes. The expected average gain $\overline{G}$ is about 10^6. The ASIC is the first version of the SPACIROC family [3]. It measures the photoelectron

[1]The "Centre National d'Etudes Spatiales" (CNES) is the French government agency responsible for the endeavour of national and international space missions.

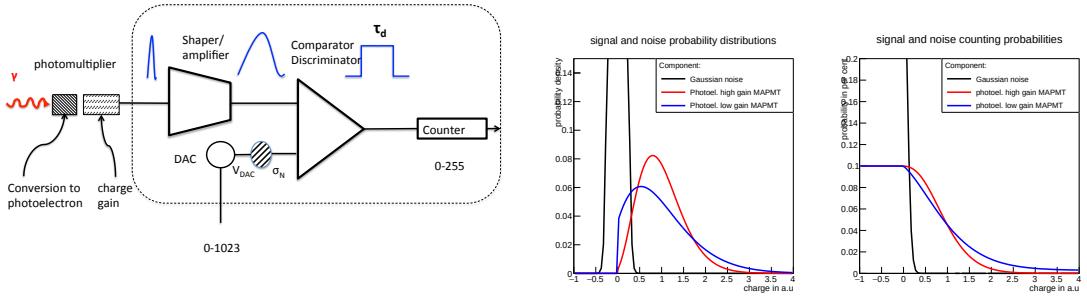

Figure 1: Left : a) Front-end electronic scheme of the PDM channels. Right: b) Expected shapes for Probability Density Function (pdf on the left) and Counting Probability Function (cpf on the right) for high gain and low gain MAPMT. The horizontal axis has been normalised to the average gain G. The photoelectron distributions (red and blue curves) are normalised to 10% of the noise distribution (black curve).

signal according to the standard photon counting method. The ASIC provides an input amplifying stage with an adjustable gain by a factor from 0 to 4 in 256 steps individually for every channel, followed by a discriminator whose common threshold voltage is controlled by a 10-bit DAC (Digital to Analog Converter). The discriminator generates digital pulses of fixed-width, which are fed to a 8-bit digital counter. The counters count the number of anode pulses above the DAC threshold during one GTU.

2.3 Signal and background model

The photoelectron amplification in the MAPMT is a complex stochastic process giving rise to a probability density function (pdf) for the signal amplitude at ASIC amplifier output, well known as the single photoelectron spectrum (SPE). The shape of this distribution has been measured experimentally [4]. It has been first calculated analytically in [5] and the theoretical result is given in the equation 1.1 of table 1. Figure 1.b) shows the pdf for noise (black) and single photoelectrons at high gain (red) and low gain (blue). If the MAPMT gain is high enough, the SPE peak is well above the pedestal level, accounting for electronic noise in ASIC electronic stages. In contrary, when the MAPMT gain is too low or the electronic noise too high, the peak value for the SPE's pdf cannot be distinguished from the electronic noise. The DAC threshold must be set to select the pulses coming from photoelectron with high enough selection efficiency and rejecting large amplitude noise fluctuations with usually negligible noise contamination. The Counting Probability Function[2] (cpf) is related to the underlying signal or noise component by its pdf integration. The cpf for signal and noise is shown on Figure 1.b) as it was calculated by numerical integration of equation 1.1 of table 1. The noise pdf is assumed to be a gaussian distribution, thus the expected cpf is given as analytical expression in equation 3.1 of table 1.

2.4 Counting saturation

In the first version of the ASIC, a dead-time of 30 ns has been introduced in the electronic

[2]The Counting Probability Function or cpf is the complement of the cumulative function of the pdf : $cpf(x) = 1 - \int_0^x pdf(y)dy$.

Analytical formula	parameters	eq. number
Probability density function (pdf) of SPE (x normalised to average gain)		
$p_G(x,a) = e^{-a}\left(\delta(x) + a\frac{e^{-ax}}{\sqrt{x}} I_1(2a\sqrt{x})\right)$	a	(1.1)
Fitted counting probability function (cpf) for SPE signal ($f(x)$, x is expressed in DAC unit)		
$f(x) = a \times \Gamma(\nu, \frac{x_{max}-x}{w})$	a, ν, x_{max}, w	(2)
Series of Fitted counting probability function (cpf) for the electronic noise ($g(x)$, x is expressed in DAC unit)		
$g(x) = a \times \mathrm{Erfc}\left(\frac{x-x_0}{\sqrt{2}\sigma}\right)$	a, x_0, σ	(3.1)
$g(x) = a \times \left[\mathrm{Erfc}\left(\frac{x-x_{01}}{\sqrt{2}\sigma_1}\right) + f \times \mathrm{Erfc}\left(\frac{x-x_{02}}{\sqrt{2}\sigma_2}\right) \times \exp\left(\frac{x-x_{02}}{\lambda_{att}}\right)\right]$	$a, x_{01}, x_{02}, \sigma_1, \sigma_2, f, \lambda_{att}$	(3.2)
$g(x) = a \times \exp - \left(\frac{x-x_0}{2\sigma}\right)$	a, x_0, σ	(3.3)
Saturation function applied to counting (h(x), where x is real counts number and $h(x)$ detected counts number)		
$h(x) = x \times \exp - \left(\frac{x}{x_{MAX}}\right)^{\alpha}$	x_{MAX}, α	(4)

Table 1: Mathematical parameterised formula used in this analysis and referred in the text. $I_1(x)$ is the modified Bessel function of the first kind. $Erfc$ is the complementary error function. $\Gamma(\nu,x)$ is the complementary Gamma function.

chain due to the finite discriminator pulse width set to match the amplifier shaping time. This dead-time leads to a disturbing saturation in photoelectron counting, thus reducing drastically the counting dynamic range to a maximum of 30 counts per GTU and paralysing the counting at high photoelectron rates[3]. This saturation combined with an electronic noise extending over a wide range of DAC thresholds makes the determination of the effective pedestal position quite difficult. In fact, the cpf for the noise should be expressed as a function $g(x)$ according the equation (3.1) in table 1. This cpf was convoluted by $h(x)$ (equation (4)), to take saturation into account. The pedestal for each channel was assessed after the flight by fitting the convoluted function to the data taken in the laboratory. The average pedestal position was found to be $x_0 = 70.69 \pm 2.56$ in DAC units.

2.5 Photoelectron peak selection and Photon Counting measurement

The photon counting method consists in setting an appropriate threshold x_{th} at the comparator, in such a way that pulses are selected with the highest electronic efficiency ε_G, and the electronic noise is highly reduced. At the low pressure of only 3 mbar in the stratosphere, the operation of the EC-units is limited to -950 V due to HV sparking and breakdown. Under these conditions, the significant overlap of the pdf with the noise peak (see blue curves of Figure 1.b) impedes the setting of an optimal threshold per pixel. In practice, the DAC threshold must be specified as number between 0-1023, proportional to the common DAC voltage of ASIC channels. During the flight, the DAC threshold $x_{th} = 250$ was chosen for the whole PDM's channels.

3. Data and Methods

3.1 Relative electronic calibration and absolute calibration

The absolute calibration is the procedure which relates the recorded pulse rate to incident photons rate in the pixels. It determines the conversion factor defined as the absolute efficiency

[3]The maximum counting rate increases from 30 counts per GTU for the SPACIROC1 ASIC to 100 counts per GTU for the SPACIROC3 ASIC.

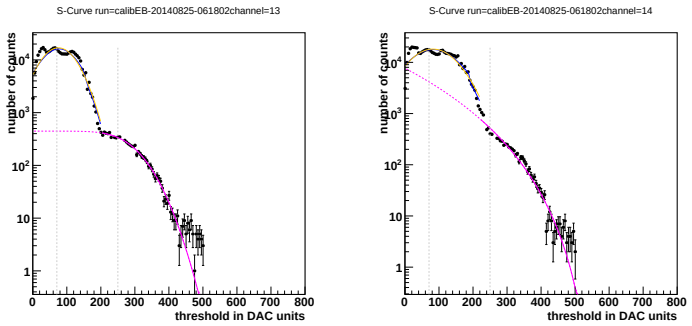

Figure 2: Example of cpf measured for two channels in one calibration run collecting 640 GTU counts per DAC threshold along the abscissa. Left : a) MAPMT high gain channel, Right : b) MAPMT low gain channel.

ε_{abs}. This procedure requires a calibrated light source to illuminate the pixels inside a black-box. It has been performed in a laboratory after the flight [6]. An in-flight calibration was not foreseen for Euso-Balloon, but it is planned for JEM-EUSO. Hence the efficiency variation during the flight could only be studied in relative electronic calibration runs which estimate $\varepsilon_G = \varepsilon_{abs}/\varepsilon_{det}$, where ε_{det} is the photon-detection efficiency (product of UV filter transparency, by photocathode quantum efficiency and primary photoelectron collection on first dynode efficiency). This article is restricted to the methods and results involved in relative electronic calibration.

3.2 Relative calibration data

The data acquisition of the PDM during the flight was operated to record series of events, each event comprising 128 consecutive GTU counts. The events were triggered at a 19 Hz rate. A DAC threshold x_{th} common to the 64 ASIC channels could be adjusted in the range 0-1023. For standard runs dedicated to photon rate measurement, $x_{th} = 250$ was set above noise level. For relative calibration runs, x_{th} was scanned from 0 up to 500 DAC units. For every threshold, the counter values were accumulated during N_{GTU}=640 cycles. The detected photons originated mostly from the irreducible sky background, known as the ionospheric nightglow reflected back from the earth ground or the clouds top to the nadir pointing telescope [7]. The photon rate during the relative calibrations runs was most of the time too low to reach counting saturation. Figure 2 shows the cpf for a typical high gain channel (left) and for a typical low gain channel (right) for a single calibration run. The right-most component of the curve is the photoelectron cpf. The wide bump on the left correspond to the pedestal component which has been widened by a number of well identified flaws in the design of the electronic hardware.

3.3 Electronic efficiency estimation

The cpf of photoelectrons can be very well fitted by the function $f(x)$ of equation (2) in table 1, for a large number of channels. The electronic selection efficiency ε_G is defined as the ratio of the fitted value of DAC threshold to the fitted value at the pedestal origin according the equation 3.1.

$$\varepsilon_G(x,x_0) = \frac{f(x,\theta_i)}{f(x_0,\theta_i)} \tag{3.1}$$

where the $\{\theta_i\}$ represents the set of the 4 fitted parameters $\{a,\nu,x_{max},w\}$. Note that x_0 is the assumed average pedestal position found by the after-flight absolute calibration.

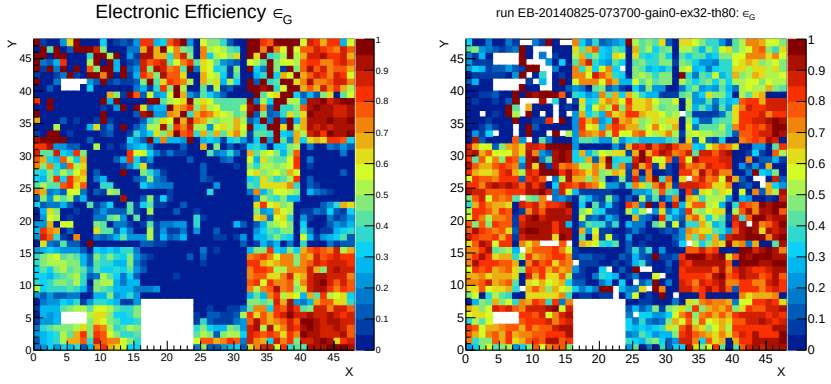

Figure 3: Left : a) Electronic efficiency map obtained with an ASIC gain common to all channels. Right : b) Electronic efficiency map after a partial gain matching inside the ASIC.

4. Results on electronic efficiencies

The electronic efficiency map averaged over periods of stable conditions is shown on the Figure 3.a). Obvious patterns linked to EC-Unit structure (16×16 pixels) and also sub-structures within EC-Units can be identified. The structural effect per EC-Unit is expected because the MAPMTs were grouped according to their gain. Good quality high gain EC-Units have ε_G values in the range 70-100%, medium quality EC-Units have ε_G values in the range 30-60% and poor gain EC-Units have ε_G values below 20%. Close to the end of the flight, an amplifier gain table had been loaded inside the ASICs. This gain table had been determined during pre-flight calibration (at nominal HV=-1100V instead of real operating HV=-950 V) to compensate for the MAPMT gain dispersion by the amplifier gains. In fact, this compensation worked only partially, as shown on Figure 3.b). Nevertheless, it improved slightly the gain equalisation over the focal surface.

The statistical errors $\sigma(\varepsilon_G)$ have been calculated from the covariance matrix of the fit parameters and the gradient of $f(x)$. The typical standard deviation error is $\sigma(\varepsilon_G) = 1\%$. For low values of ε_G less than 5%, the estimations of ε_G are not reliable anymore because $\sigma(\varepsilon_G) > \varepsilon_G$. The systematics errors can be estimated from the variability of ε_G during the flight by 20%. This is comparable with the post-flight calibration. These variabilities were caused by an under-voltage in some ASICs caused by a higher than expected power consumption of some ASICs during the flight.

5. Results on electronic background

In order to estimate the average background $\bar{b}$ per GTU, the pedestal component shown in Figure 2 has to be extrapolated at the DAC threshold $x_{th} = 250$. As no physical model really describes this kind of background, three equations (3.1),(3.2) and (3.3) of table 1 have been tried to fit the pedestal component. As some functions failed to model the noise and others could not be fitted, we finally selected a function per pixel with the lowest χ^2 per degree of freedom. Then the average background is

$$\bar{b} = \frac{g(x_{th})}{N_{GTU}} \tag{5.1}$$

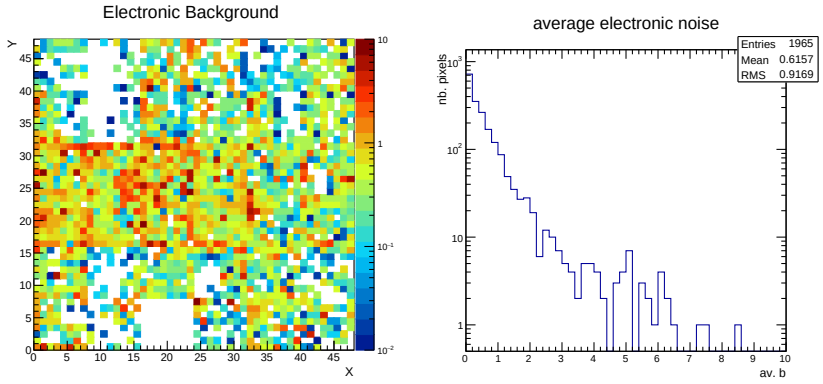

Figure 4: Left a) Map of average noise count per GTU $\overline{b}$ during flight. Right : b) Distribution of $\overline{b}$ over channels.

with $N_{GTU} = 640$ being the number of cumulated GTU counts per DAC levels in the calibration runs. Figure 4.a) shows the pixel-map of the estimated electronic noise $\overline{b}$. The average noise is about 0.6 ± 0.9 counts per GTU, with a few channels above one count. The noise doesn't seem to be related to any structural effect of the PDM electronics. But it is related to bad electrical connections inducing a bad ground return path between the MAPMT and the ASICs. The relative statistical error on $\overline{b}$, calculated from the parameters covariance matrix and $g(x)$ parameters's gradients, is of the order of a few percents. It must be emphasised that the electronic noise could be greatly reduced at post-flight ground calibration such $g(x_{th}) = 0$ for a number of cumulated GTU, $N_{GTU} = 3200$. On ground, the upper limit on the electronic noise was $\overline{b}^{ul} = 0.00075$ counts per GTU at 90% confidence level (CL,[8]), thus 3 order of magnitude less than the flight's upper limit.

6. Detection sensitivity

The detection sensitivity is the minimum photoelectron rate (on the first dynode) which can be detected at 90% CL. It is calculated by dividing the average upper limit at 90% CL on the noise-induced counts rate by the electronic efficiency. The sensitivity map in Figure 5.a) shows the same structural pattern as the efficiency map in Figure 3.a). The corresponding sensitivity distribution over all pixels is shown on Figure 5.b). The average sensitivity in the *p.e.* per GTU range 1-100 is 8 *p.e.* per GTU and the peak sensitivity is 3 *p.e.* per GTU. For comparison, the sensitivity calculated from low electronic noise of post-flight ground calibration is 0.0008 *p.e.* per GTU, thus better by more than 4 orders of magnitude.

7. Conclusions and perspectives

This article presented the photoelectron detection performance of the Euso-Balloon UV camera during the first balloon flight. The electronic efficiencies and the detection sensitivity could be estimated from the single photoelectron spectrum recorded in the relative calibration runs. As the operating conditions were far from optimum during the flight, a large spread over the pixels has been obtained on those parameters. The detection performances on post-flight data, much less

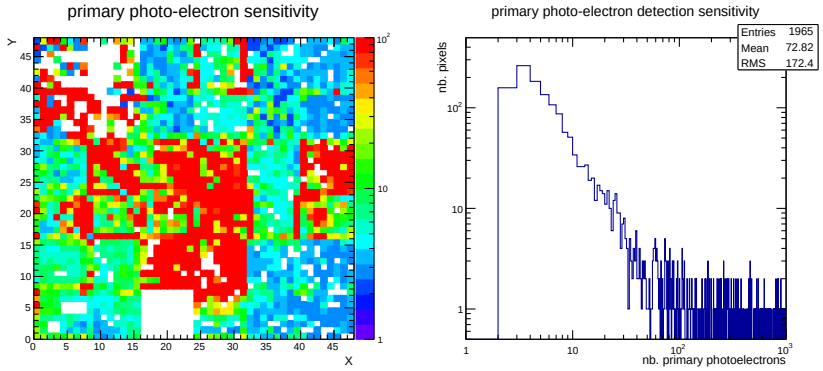

Figure 5: Left : a) Map on the sensitivity on the number of primary photoelectrons per GTU .Right : b) Distribution on the sensitivity on the number of primary photoelectrons per GTU over pixels.

affected by electronics noise, resulted in a significant improvement by 3 to 4 orders of magnitude in detection capabilities. These good results encourage us to conduct further balloon flights. After having fixed the few identified flaws in the hardware, we expect to achieve a detection performance much closer to our original expectations.

Acknowledgment: The authors gratefully acknowledge CNES, the French National Space Agency, for its strong support on the JEM-EUSO and Euso-Balloon. Its encompasses its funding contribution in the ASIC SPACIROC development, its funding of the Euso-Balloon project but also for its valuable technical help all along the Euso-Balloon project development phases and also during the final CNES balloon flight in its Timmins Canadian stratospheric balloon base in 2014. Without this strong support all reported work would not have been possible.

References

[1] P. von Ballmoos et al., *General overview of EUSO-BALLOON mission*, in proceedings 0735 of the *34th ICRC2015*,PoS(ICRC2015)725 (2015)

[2] Mario Bertaina et al.,*Preliminary results from the EUSO-Balloon flight*, in proceedings 890 of the *34th ICRC2015*,PoS(ICRC2015)890 (2015)

[3] Salleh Ahmad, *Développement et réalisation d'un circuit de microélectronique pour le détecteur spatial de rayons cosmiques JEM-EUSO*, University Paris-Sud (Paris 11), PhD-thesis(2012), LAL 12-412

[4] Carl Blaksley, *Photodetection Aspects of JEM-EUSO and Studies of the Ultra-High Energy Cosmic Ray Sky*, University Paris Diderot (Paris 7), PhD-thesis, APC-2013

[5] H.H. Tan, *A statistical Model of the Photomultiplier Gain Process With Applications to Optical Pulse Detection*, *TDA Progress Report* **42-68** (1982)

[6] Camille Moretto et al. , *Absolute Calibration of the Photo Detector Module of the Euso-Balloon experiment and improvements for future missions*, in proceedings 1016 of the *34th ICRC2015*, PoS(ICRC2015)1016 (2015)

[7] Simon S. Mackovjak et al. *Night Time Measurement of the UV Background by EUSO-Balloon*, in proceedings 1302 of the *34th ICRC2015*,PoS(ICRC2015)1302 (2015)

[8] Gary J. Feldman and Robert D. Cousins, *Unified approach to the classical statistical analysis of small signals*, *Phys. Rev.* **D 57, 3873 (1998)**